1.0
1.1
1.25 1.4 1.6

3.2
3.6
4.0

2.2
2.0
1.8

2.4
2.5

MIC

DTIC FILE COPY SC5398.4FR

Copy No. 44

SC5398.4FR

AD-A178 744

METALLIDING AS AN ELECTROCHEMICAL PROCESS

FINAL REPORT FOR THE PERIOD
June 1, 1984 through November 30, 1986

CONTRACT NO. DAAG29-84-C-0006

Prepared for

U.S. Army Research Office
P.O. Box 12211
Research Triangle Park, NC 27709

M.W. Kendig
D.O. Raleigh
Principal Investigators

DTIC
ELECTE
APR 2 1987

A

JANUARY 1987

Approved for public release; distribution unlimited

The view, opinions, and/or findings contained in this report are those of the author(s) and should not be construed as an official Department of the Army position, policy, or decision, unless so designated by other documentation.
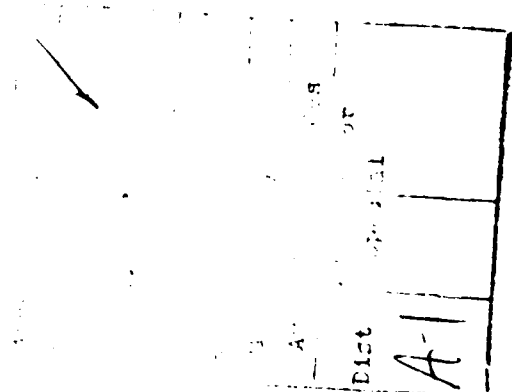
Rockwell International
Science Center

87   4   1   3 15

REPORT DOCUMENTATION PAGE

1a. REPORT SECURITY CLASSIFICATION UNCLASSIFIED	1b. RESTRICTIVE MARKINGS
2a. SECURITY CLASSIFICATION AUTHORITY	3. DISTRIBUTION/AVAILABILITY OF REPORT Approved for public release; distribution unlimited
2b. DECLASSIFICATION/DOWNGRADING SCHEDULE	

4. PERFORMING ORGANIZATION REPORT NUMBER(S) SC5398.4FR	5. MONITORING ORGANIZATION REPORT NUMBER(S) ARO 21289.3-MS

6a. NAME OF PERFORMING ORGANIZATION ROCKWELL INTERNATIONAL Science Center	6b. OFFICE SYMBOL (If applicable)	7a. NAME OF MONITORING ORGANIZATION

6c. ADDRESS (City, State and ZIP Code) 1049 Camino Dos Rios Thousand Oaks, CA 91360	7b. ADDRESS (City, State and ZIP Code)

8a. NAME OF FUNDING/SPONSORING ORGANIZATION U.S. Army Research Office	8b. OFFICE SYMBOL (If applicable)	9. PROCUREMENT INSTRUMENT IDENTIFICATION NUMBER Contract No. DAA29-84-C-0006

8c. ADDRESS (City, State and ZIP Code) P.O. Box 12211 Research Triangle Park, NC 27709	10. SOURCE OF FUNDING NOS.			
	PROGRAM ELEMENT NO.	PROJECT NO.	TASK NO.	WORK UNIT NO.

11. TITLE (Include Security Classification)
METALLIDING AS AN ELECTROCHEMICAL PROCESS

12. PERSONAL AUTHOR(S)
M.W. Kendig and D.O. Raleigh

13a. TYPE OF REPORT Final Report	13b. TIME COVERED FROM 06/01/84 TO 11/30/86	14. DATE OF REPORT (Yr., Mo., Day) January 1987	15. PAGE COUNT 44

16. SUPPLEMENTARY NOTATION
The view, opinions, and/or findings contained in this report are those of the author(s) and should not be construed as an official Department of The Army position, policy, or decision, unless so designated by other documentation.

17	COSATI CODES		18. SUBJECT TERMS (Continue on reverse if necessary and identify by block number)
FIELD	GROUP	SUB. GR.	Metalliding, surface modification, molten salts, aluminum, carbon steel,
			titanide wear, corrosion resistance, ceride, boride

19. ABSTRACT (Continue on reverse if necessary and identify by block number)

Controlled electrolysis in molten salts can improve the surface properties of metal alloys for wear and corrosion resistance. Surfaces of aluminum 1100 and carbon steel were modified by passage of cathodic current under potentiostatic and galvanostatic control in molten salts variously containing Ce^{3+}, BF_4^-, Ti^{3+} ions. Hard, poorly adherent $CeAl_4$ and $CeAl_3$ layers formed on Al surfaces at potentials which were some 200 to 400 mV positive to the reduction potential of Ce. The deposition occurred by a reductive precipitation mechanism from a KCl/LiCl melt at 560° C containing 1 mole% Ce^{3+}. Boride and titanide layers were formed on steel in a LiF/KF melt containing the respective ions. A borided layer on steel exhibited a factor of ten improvement in hardness and a titanided layer exhibited a 30% increase in hardness. While the borided steel showed only marginal improvement over the substrate in resistance to corrosion in neutral aerated 0.5M NaCl, the titanided steel showed a significant improvement in corrosion resistance under these conditions.

20. DISTRIBUTION/AVAILABILITY OF ABSTRACT UNCLASSIFIED/UNLIMITED ☐ SAME AS RPT. ☐ DTIC USERS ☐	21. ABSTRACT SECURITY CLASSIFICATION UNCLASSIFIED	
22a. NAME OF RESPONSIBLE INDIVIDUAL	22b. TELEPHONE NUMBER (Include Area Code)	22c. OFFICE SYMBOL

Handwritten annotations on abstract: Ceric aluminide; Cerous aluminide; Sodium chloride; Cerium(3+); Boron tetrafluoride(-); Titanium(3+)

TABLE OF CONTENTS

Page

SC5398.4FR

LIST OF FIGURES

LIST OF FIGURES

1.0 INTRODUCTION – BACKGROUND AND OBJECTIVE

Adverse environmental effects, economic factors, and structural demands often place seemingly incompatible requirements on materials used in environments of high corrosivity or wear. High-performance coatings can meet these demands. Particularly useful are coatings that fall into the category of "surface modification" such as nitriding or carburizing. Surface modification is distinguished from conventional coatings in that the surface layer is formed by in-situ conversion of the workpiece surface to a new alloy or compound. Surface modification eliminates many problems, such as cracking, spalling and pinholing, that are associated with physically distinct coating layer formation.

The metalliding surface modification process,[1-5] developed in the 1960's by N. Cook,[1] entails the electrodeposition of a metal from a molten halide bath in the form of a surface alloy with the substrate metal. The mechanism for this process involves the following reactions:

$$\underline{\text{anode (metallide metal M(1))}}: \quad M(1) \rightarrow M(1)^{n+}_{melt} + ne- \tag{1}$$

$$\underline{\text{cathode (workpiece metal M(2))}}: \quad ne^- + M(1)^{n+}_{melt} \rightarrow M(1)_{surface\ of\ M(2)} \tag{2}$$

$$M(1)_{(surface\ of\ M(2))} \rightarrow (diffusion) \rightarrow M(1)\text{-}M(2)\ alloy \tag{3}$$
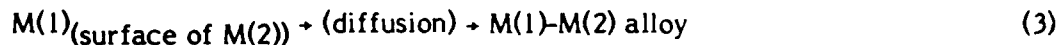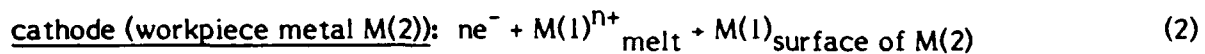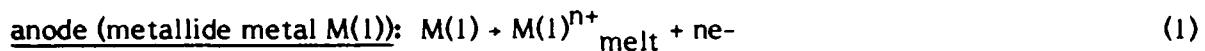
For the metalliding process to proceed, the side reaction:

$$M(2) \rightarrow M(2)^{m+}_{melt} + me- \tag{4}$$

must be substantially less favorable than reaction (2). This can be assured by:

1. Solid solubility of M(1) in M(2)

2. The relative stability of the fluoride of M(1) over that for M(2).

3. M(1) being more electropositive than M(2)

Criteria 2 and 3 have led to a metalliding series which orders metals with respect to their ability to metallide metals below them in the series.[1,4] Y, Ce and the transuranic elements reside at the top of the list, while the noble metals remain near the bottom.

Even for cases where all of the above criteria are met, slow rates for any of the steps may adversely affect the viability of the process. For example, a slow diffusion process brought about by the presence of substrate impurities or a slow rate of alloying will minimize the kinetics of reaction (3). On the other hand, less electropositive metals can metallide more electropositive metals in cases where alloy formation is highly favored, provided the substrate is introduced to the melt under applied potential.

Typically, metalliding has been carried out under constant current conditions. Accordingly, the potential at the substrate cathode will change with time as the alloy composition gradually increases toward that of pure M(1), at which point conventional electroplating commences. However, if the process were carried out under potential control, and in the absence of or correction for ohmic potential drop within the melt, a given alloy composition could be maintained at the surface as the metallide metal diffuses into the bulk. In this case, the activity, a_m, of the diffusing metal at the surface remains constant according to the equation:

$$a_m = \exp(-(nFE/RT) \tag{5}$$

where E is the difference between the potential of the substrate and the reversible potential of a nonpolarized reference electrode of the metallide metal. The current for this reaction would follow the equation:

$$i = FAC_m(D/\pi t)^{1/2} \tag{6}$$

where C_m is the surface concentration of the diffusing metalliding element.

Fluoride melts provide an execellent medium for metalliding as a result of their ability to dissolve residual layers of the surface oxides on the substrate materials.[1,2,4]

As a structural material, Al finds increased application due to its relatively low density. However, it is a soft, easily scratched metal, and corrosion, wear and

fatigue limit its ultimate usefulness. A rapid, economical method for hardening the surface of Al components against corrosion and wear without altering the fabricated surface geometry would benefit a number of technologies associated with vehicle construction where adverse environmental effects demand high corrosion or wear resistance.

It has been the objective of this project to provide the electrochemical characterization required to make metalliding a reliable well-understood and well-controlled process for metal surface modification, and to explore the possibility of producing a hard, corrosion-resistant metallide surface on Al.

Metalliding Al with a number of elements should be possible, despite its high electropositive ranking and its tendency to form extremely stable oxides that persist to low levels of residual oxygen, which could inhibit the diffusion of metallide metals. Since the halide of the metalliding metal must have greater stability in the melt than the halide of the substrate, in addition to being more electropositive for metalliding to occur, the metals Ce, Sc, Hf, Zr and Ti (as shown in Table 1) would be expected to form a metallide in fluoride, given their fluoride stabilities, electropositive nature and solubility in Al. K, of course, is completely insoluble in Al, and therefore would not metallide despite its electropositive nature and stable fluoride. Ce, the most electropositive of the metals considered, was chosen as a first candidate for metalliding Al. It lies substantially above Al in the metalliding series,[4] and several obscure reports have been made of the successful ceriding of Al from a chloride melt.[6] Experiments were conducted to evaluate the ability of Ce to metallide Al from KCl/LiCl and KF/LiF melts.

Table 1

Thermodynamic Data for Metallurgical Reactants

Metallide Metal	Free Energy of Formation of the Fluoride $1000° = \Delta G_{F_{kcal/mol}}$	Electronegativity (Pauling)	ϵ_0^{25*} (Volt)	Solubility M in Al
Ce	-115	1.1	2.48	.05 wt%
Y	-110	1.2	2.37	0.8 wt% at eutectic temp.
K	-101	0.8	2.95	Insoluble
Sc	- 98	1.3	2.08	~ .05 at. %
Hf	- 93	1.3	1.70	0.182 at. % at 662°C
Zr	- 92	1.4	1.53	0.068 at. % at 640°C
Ti	- 90	1.5	1.63	0.14 at. % 665°C
Al	- 89	1.5	1.66	n.a.

n.a. Not applicable

* $M^{n+} + ne^- = M$ (aqueous)

2.0 SUMMARY OF RESULTS

This work has concentrated on ascertaining the feasibility of hardening Al and steel by the electrochemical surface modification process of metalliding in a molten salt electrolyte. Intermetallic Al-Ce compounds of $CeAl_4$ and $CeAl_3$ were found to form at 560°C in LiCl/KCl electrolytes at 350-450 mV more positive than the potential for the reduction of Ce. The resulting film is 20-50 times harder than Al, but shows poor adhesion to the Al surface. The formation mechanism most likely entails the reductive precipitation of the material from the melt. Solid solution does not form under the conditions due to low solubility and diffusion of Ce into Al. A possible means for forming a hard Ce on Al might result from hot-dipping of Al into the 580°C, 95% Ce-5% Al eutectic. Further investigation into this possibility is recommended. While a poorly adherent intermetallic film forms on Al, an adherent diffusion layer of Ce readily forms on Pt.

Titanide compounds formed on steel from a LiF/KF melt 1 mole% in TiF_3 melt, but did not form on Al due to the fact that Al is much more active than Ti in the fluoride melt. Steel coated with Ti compounds at 744°C exhibited greatly reduced corrosion in stagnant room-temperature 0.5 M NaCl compared to 4340 steel in this medium. The titanided steel surface was 30% harder than the substrate.

Galvanostatic polarization of steel in a 3.5 mole% BF_4^- in molten LiF/KF at 866°C converts the surface to a boride, which is 10 times harder than the steel substrate, confirming the work by others. The borided steel surface exhibits an invariant (over 48 h) corrosion rate of about 20 $\mu A/cm^2$ in stagnant room-temperature 0.5 M NaCl, comparable to 4340 steel. Time dependence of the capacitance and corrosion potentials for the borided steel, however, indicate the formation of a film on the borided surface which might provide an inhibiting effect for times in excess of 48 h.

The ease of formation and hardness of the borided steel recommends it as a viable process for protecting critical structural surfaces from degradation due to wear. On the other hand, Al in the boron-containing electrolyte corrodes too rapidly to allow successful boriding to take place.

Metalliding of the less electropositive metals such as Fe and Pt can readily be performed electrochemically in molten salt electrolytes. It is difficult to form metallides on the highly electropositive metals such as Al due to its activity in the molten salt.

For all systems considered, the relatively high solution resistance of the molten salts make accurate potentiostatic control of the metalliding process difficult. In performing controlled potential metalliding, the ohmic drop must be considered, as it is very significant.

3.0 EXPERIMENTAL

3.1 Apparatus

Figure 1 shows a schematic for the apparatus used in the metalliding experiments. A quartz cell sealed with an elastomeric gasket formed the outer cell which was placed in a thermally controlled furnace. The cell contained an alumina crucible that held the fused salt. A number of stainless steel baffles placed above the salt container minimized heat loss from the cell, thereby protecting the gaskets of the cell cap and electrode fittings. The electrodes and thermocouple well passed through holes in the baffles, and could be lowered into the melt by loosening gasketed compression fittings and pushing the respective electrodes of the thermocouple well down into the melt. The cell atmosphere could be controlled from a 5 mTorr to 3 psi atmosphere of high purity (< 1 ppm O_2) Ar, as shown in Fig. 1. Vented gases were directed through an O_2 meter, followed by an oil-seal for minimizing any backdiffusion of atmospheric oxygen. A potentiostat was used to control the potential of the specimens (M_2) vs a reference electrode (M_3). A second electrode (M_1) served as the auxiliary electrode and anode during the metalliding process. Additional apparatus in the form of a computer-controlled transfer function analyzer (TFA) or a sweep generator (not shown) could be used in conjunction with the potentiostat for respectively collecting the electrochemical impedance spectrum or cyclic voltammograms. A PAR model 373 served for most of the metalliding runs. For tests using IR compensation, the Stonehart BC1200 potentiostat was used with IR compensation via positive feedback. For the impedance measurements, a PAR 173 with a model 276 interface was used, as described elsewhere.[7]

3.1.2 Melt Preparation

3.1.2.1 KCl/LiCl Melt Containing Ce

107 gm of Anderson Physics Laboratories (APL) LiCl/KCl eutectic, 2.95 gm of $CeCl_3$ and 1 gm of Ce chips (Alfa 99.9%) were weighed out and transferred to the crucible and sealed in the cell in a dry Ar atmosphere. The Ce electrodes (Alfa 99.9%) were abraded in the dry Ar atmosphere and connected to stainless steel leads running through Al_2O_3 rods, which were sealed at the outer end with a hard wax.
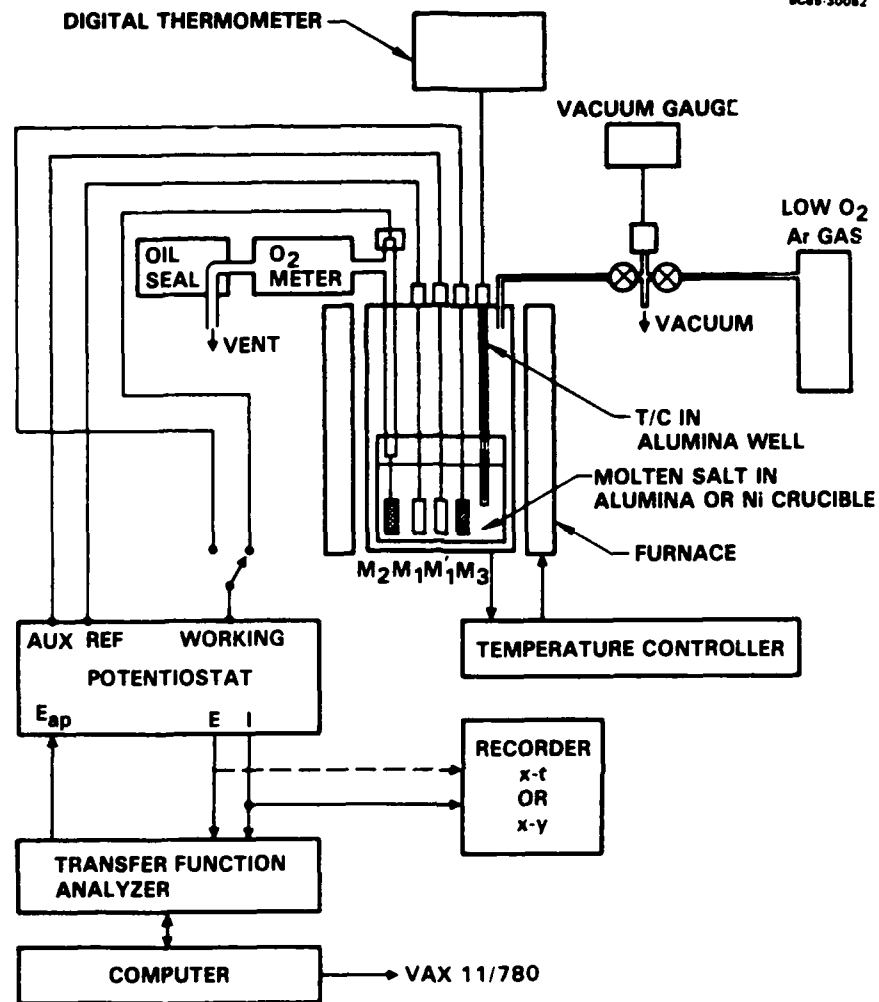
Fig. 1 Schematic of the apparatus.

The cell containing the electrodes and salts was transported to the furnace and slowly raised to 560°C with no further purification.

3.1.2.2   KF/LiF Melts Containing Ce

16.85 gm of LiF (Reagent grade Anachemia AC 5469) 37.02 gm of KF (Aldrich, 99.999%), and 2.07 gm $CeCl_3$ (corresponding to 1 mole%) were weighed out in a dry Ar atmosphere and were transferred to the melt crucible. The crucible was slowly heated to 550°C under vacuum to remove residual water and then was allowed to cool. Ce chips were added and the system was elevated to 610-620°C for the metalliding. The vacuum

treatment was necessary to remove residual water from the melt. Above ~ 600°C, a vacuum could not be applied to the system since it caused decomposition of the melt, forming K vapor. The vapor condensed on the cold portions of the cell and was later confirmed to be K from a flame test. A second fluoride melt was made up in the same manner, except that 1 m/o of CeF_3 (Aldrich 99.9%) was used in place of $CeCl_3$ and the 99.9% Ce was obtained from Goodfellows.

3.1.2.3   KF/LiF Melt Containing Ti

A Ni crucible contained 44.4 g (1.7 moles) of LiF and 91.8 g (1.58 moles) of KF. 1 mole% (0.033 moles) of TiF_3 was added to these salts. The crucible was filled and placed in the cell in a glovebox purged with Ar. The cell was then placed in the furnace and connected to the system in Fig. 1 and evacuated at 60°C and 200 mTorr. The temperature of the evacuated cell was gradually increased to 100°C to drive water from the salts. After being evacuated for 24 h, the salts were brought to a working temperature of 560-600°C for the metalliding experiments. Ti served as the reference (M_1) and counter (M_1') electrodes.

3.1.2.4   KF/LiF Melt Containing B

In a Ni crucible in a glovebox purged with Ar, 1.8 mole LiF, 1.8 mole KF and 0.133 mole KBF_4 were weighed. The crucible was placed in the cell (Fig. 1) and sealed. The cell was attached to the system in Fig. 1, evacuated and slowly heated to 467°C keeping the pressure under 100 mTorr. The heat was removed and the cell kept under vacuum for 16 h before bringing to temperature for the metalliding experiments. Boron chips held in an Au basket served as the counterelectrode (M_1'), and a graphite thermocouple well was used as the pseudo-reference electrode (M_1).

3.1.3   Metallography and Specimen Analysis

Selected specimens were subjected to scanning electron microscopic analysis (SEM), including x-ray fluorescence analysis (EDAX). The loosely adhering scale was removed from the surface by light abrasion and was mounted in the microscope for this analysis. In several instances, metallographic cross sections of the treated specimens were mounted in epoxy and were polished to 0.03 µm finish in kerosene, followed by an

electropolish in $MeOH/H_2SO_4$. Optical micrographs and hardness measurements were obtained for the cross sections.

For one case where a metallic scale was formed on the specimen, the scale was stripped from the specimen and was mounted with double-sided adhesive on a glass slide for x-ray diffraction.

3.1.4   Electrochemical Analysis

Electrochemical impedance measurements were performed on Al test specimens, using techniques described in Ref. 7 and references therein.

4.0 RESULTS

4.1   Formation of Ce Coatings

4.1.1   Chronoamperometry in Cl⁻ and F⁻ Melts

Figure 2 compares currents (i) vs time (t) behavior of Al specimens in KF/LiF and KCl/LiCl melts at various applied potentials with a calculated plot computed from Eq. (6), assuming a solid-state diffusion coefficient of 10^{-10} cm^2 s^{-1} and a surface activity of 0.9. The calculated curve represents an upper limit for the metalliding currents. However, the i-t curves in both Cl⁻ and F⁻ melts show higher currents. The currents are typically much higher in the F melt and decrease erratically with time. The nonlinear behavior of the current as a function of $t^{-1/2}$ suggests Al-Ce compound formation rather than Ce diffusion. The behavior in the Cl appears to be diffusion-limited with $t^{-1/2}$ dependence. Previous investigators claimed ceriding Al gave better results with the Cl⁻ compared to the F⁻ melt.[5]
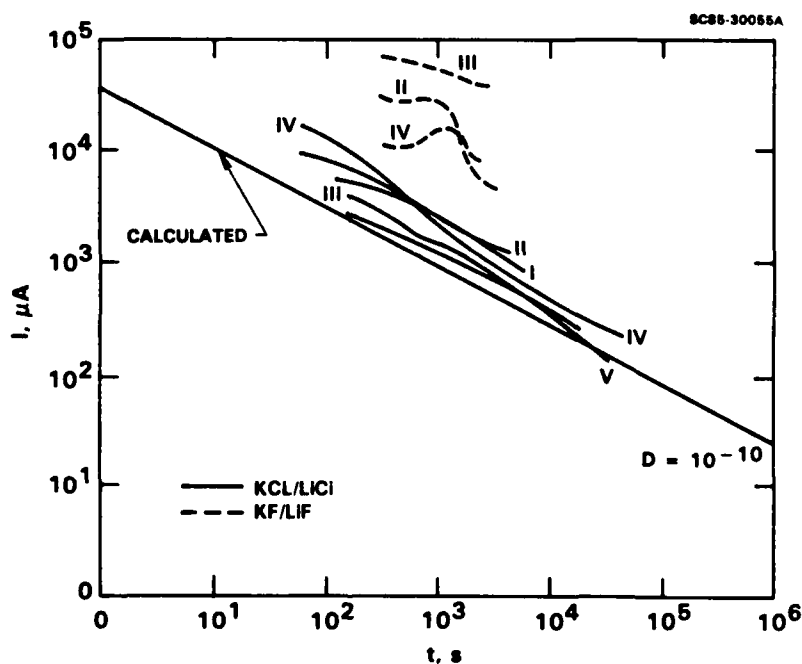

Fig. 2   Typical log current vs log time curves for specimens treated in KCl/LiCl at 560°C and 2.5 mV (I, II, III); 16.5 mV (IV, V); in the KF/LiF melt between 580-615°C at 2.5 mV (II); 16.5 mV (III) and 35 mV (IV) compared with a calculated curve.

4.1.2 Impedance Analysis

Changes in the resistance of surface films and relative reaction rates at Al electrodes were monitored with electrochemical impedance spectra.[7-9] Impedance spectra for Al 1100 in the Cl^- and F melts are shown in Fig. 3. The spectra allow evaluation of the polarization resistance, R_p, and the apparent solution resistance, R_s. R_p equals the low-frequency limit of the impedance spectrum minus R_s obtained from the high-frequency limit. R_p relates inversely to the rate of charge transfer at the metal/ electrolyte interface, and R_s depends on the combined resistance of the solution and the inhibiting films. The spectrum for the Al in the chloride medium can be resolved into a nonzero R_p of 82 Ω and an R_s of 0.35 Ω for the ~ 2 cm^2 specimen. No R_p could be resolved for the F^- melt, since R_p is substantially less than the R_s of 3 Ω as a result of a rapid charge transfer reaction, possibly due to corrosion. The decrease in R_s for the Cl^- melt compared to the F^- melt of nearly an order of magnitude suggests a higher solution resistance for the higher melting F^- salt. On the other hand, R_p for Al in the Cl^- melt is between one and two orders of magnitude higher than for the F^- melt, suggesting a lower corrosion rate, possibly due to the presence of residual surface oxides in Al. Thus, the F^- melt can dissolve residual surface oxides on substrates, but provides an ironically more resistive medium.

Impedance spectra obtained for Al and Pt in the $CeCl_3$-LiCl/KCl eutectic after various electrochemical treatments appear in Fig. 4. Curves 1 and 2 compare the response at Pt and Al electrodes, with roughly the same surface area and geometry relative to the Ce counter and reference electrodes, and thus the same R_s. Significantly higher R_s for Al suggests the presence of resistive films on the surface. The low-frequency portion of the impedance spectra results from interface charging. The large rise in impedance for Pt at frequencies < 100 rad/s indicates a low exchange current density. Due to the noble nature of Pt, no processes exist at open circuit which provide a reversible depolarization. The polarization resistance for Pt is on the order of 10^4 Ω for the ~ 2 cm^2 electrode. In the same frequency regime, a lower impedance on the order of ~ 10^2 Ω is observed for Al, Curve 2, which implies a greater exchange current density at open circuit by a factor of 100 due to the active dissolution of Al. The impedance for Al is further lowered when the electrode is potentiostatically cycled in the melt, Curve 3, and after prolonged electrolysis at 250 mV vs Ce, Curve 4, implying formation of a more rapidly depolarized interface.

SC85-30061
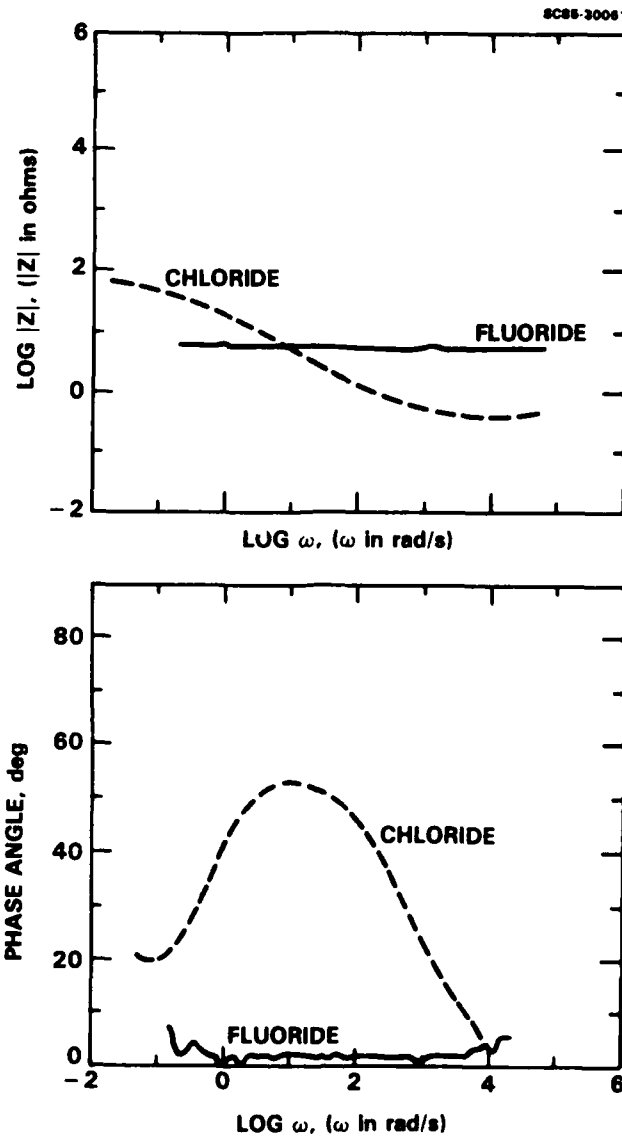
Fig. 3 (a) Electrochemical impedance, and (b) phase angle spectra for Al 1100 in LiCl/KCl melt at 560°C and LiF/KF melt at 610°C.
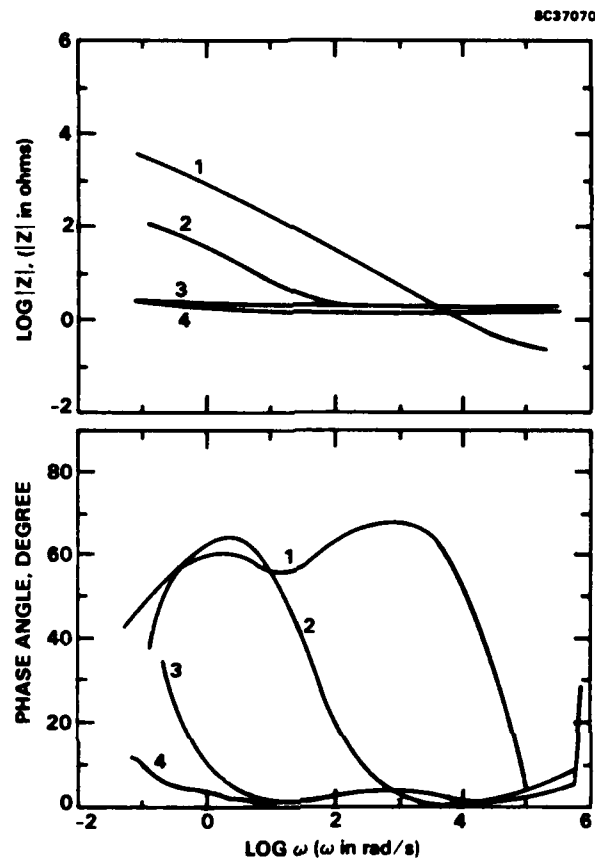
Fig. 4   Comparison of (a) impedance and (b) phase angle spectra for Pt (1), Al (2), Al after voltammetric cycling (3) and Al after 15 h electrolysis at 0.25 V vs $E_{Ce^{+3}/O}$ (4).

Impedance measurements were routinely used to monitor the electrode surface condition before and after metalliding runs in the melt.

4.1.3   Voltammetric Analysis in Cl⁻ Melt

The current-voltage (I-V) behavior at a Pt electrode was initially examined to establish the voltammetric characteristics of the melt, and also to provide a frame of reference for Al-based experiments. Figure 5 shows cathodic current peaks (a, b and c) for Pt. The magnitude of the currents and the fact that these peaks reproduce on cycling suggest that they involve formation of Pt cerides rather than reduction of Pt oxides. On the other hand, metallic Ce deposits reversibly at potentials slightly positive of 0 V,
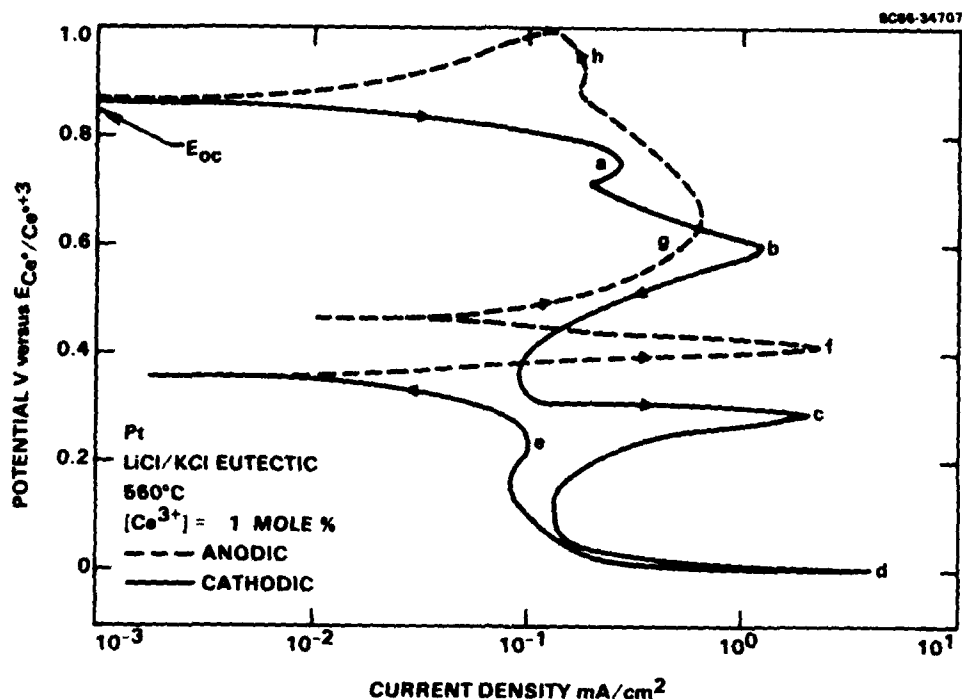
Fig. 5   Controlled potential polarization curve in a LiCl/KCl eutectic melt containing 1 mol% CeCl₃ for a Pt electrode; scan rate 0.2 mV/s.

region d. Peaks c and e probably correspond to the same reaction. The anodic peak f appears to be stripping of Ce metal plated at peak d. Peaks g and h may involve oxidation of Pt cerides formed at peaks a, b and c.

Figure 6 shows a comparable experiment for an Al electrode. The open circuit potential (E_{oc}) of 0.47 V is less than that for Pt. The two reduction waves a and b, as in the case of Pt, appear to involve formation of Ce-Al compounds. The partial current discontinuity at 0.12 V implies passivation of the surface, possibly by the formation of a diffusion-limited Ce-Al film. Ce plating occurs at d and its dissolution is represented by the sharp anodic peak at f. Processes c and e are probably related as are b and g, and a and h. Note that unlike the Pt case, g and h are cathodic processes. This behavior is reproducible for freshly polished Al electrodes.

Following the experiment in Fig. 6, subsequent cyclic voltammograms for an "aged" Al electrode differ in the definition and magnitude of the current peaks and the shift in E_{oc}, as shown in Fig. 7. The high anodic currents i and j probably involve oxidation of the Al cerides or formation of AlCl₃, causing a positive shift in the E_{oc}.

Fig. 6   Experiment of Fig. 5 at an Al electrode; initial trace.

Fig. 7   Anodic and cathodic voltammetric scans at an Al electrode precycled in the melt as in the experiment of Fig. 6.

The differences in peaks a and b between initial (Fig. 6) and subsequent (Fig. 7) scans may be attributed to the nucleation of a new Ce-Al phase on a fresh Al surface for the former case.

The various voltammetric features diminish or disappear when the scan rate is increased by one or two orders of magnitude, as shown in Fig. 8 by Curves 1 and 2, respectiv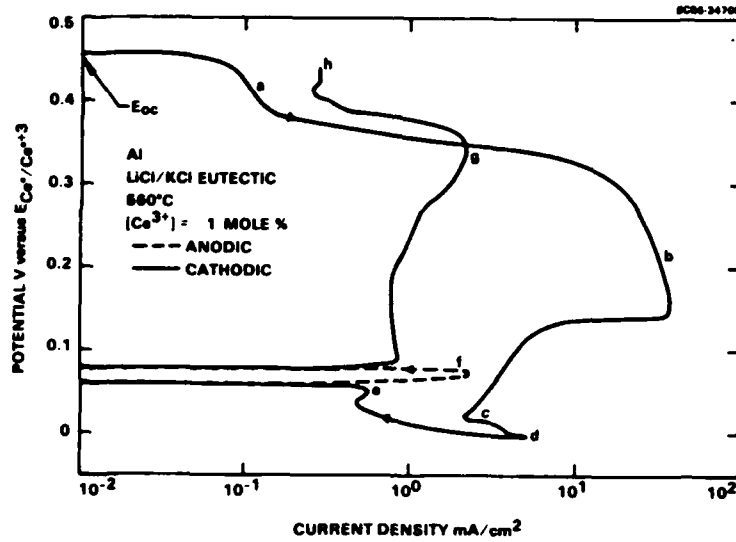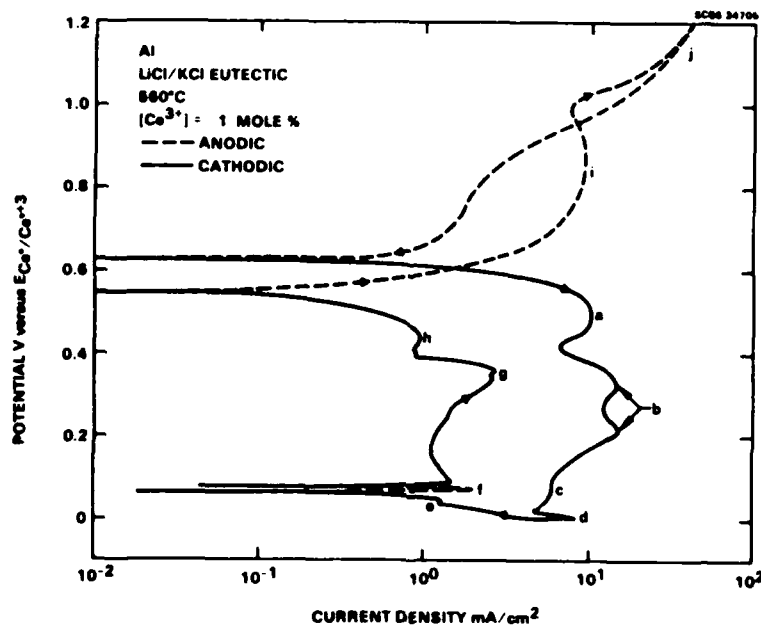ely. Curve 1 retains some structure, while Curve 2 is featureless and exhibits nearly reversible Tafel slopes. These results suggest that intermetallic diffusion is too slow to attain equilibrium under these conditions, and to allow formation of Al-Ce compounds or alloys.

The voltammetric features change as the bath becomes more "active", as shown in Fig. 9. At present, it is unclear whether the increased surface activity was caused by the presence of dissolved Al(III) (generated during anodic cycles) or by the changes in temperature between runs. The E_{oc} is more negative than in Fig. 6 and fluctuated between 250-350 mV vs $E_{Ce/Ce^{+3}}$. Cathodic traces initiated at E_{oc} show net anodic currents, except for a brief cathodic transition b, and the Ce deposition current g. The transitions b, d, e, f and i correspond to processes described in Fig. 6. A negative shift in the overvoltage for the anodic reaction i appears to result in superimposition of anodic and cathodic currents yielding a net current observed in Fig. 9.

4.1.4   X-Ray Diffraction of Cerided Al

Visual inspection of Al specimens polarized at 250 mV vs $E_{Ce/Ce^{+3}}$ for up to 15 h discerned formation of a grey-black film which was not always adherent to the substrate. Some of these films were mechanically removed and characterized with x-ray diffraction. The diffraction pattern shown in Fig. 10 identifies the film as comprising mainly $CeAl_4$, with some $CeAl_3$ and α-Ce.

4.1.5   Photomicrographs

Cross sections of specimens subjected to different electrochemical treatments were examined optically and also tested for hardness. Photomicrographs in Fig. 11 illustrate the formation of different layers and the range of adhesion encountered for the various cerided Pt and Al samples. Micrographs (a) and (b) were obtained on Pt and Al
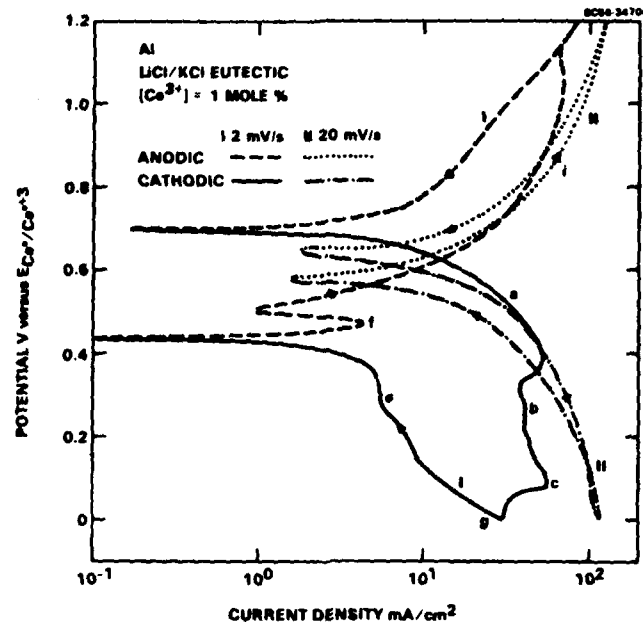
Fig. 8 Experiment of Fig. 7 at scan rate of (I) 2 mV/s and (II) 20 mV/s.
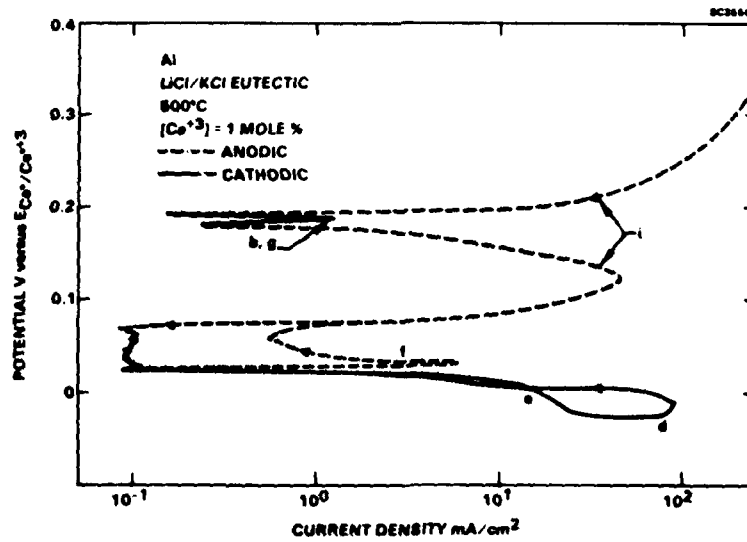
Fig. 9 Experiment of Fig. 6 in an aged melt.

Fig. 10   X-ray diffraction for the surface layer formed from electrolysis at 0.25 V vs Ce in Ce-LiCl/KCl eutectic at 560°C.

samples after cyclic polarization between E_{oc} and 0 V vs $E_{Ce/Ce}{}^{+3}$ (cathodic polarization only) as in Figs. 5 and 6. Conversion of the Pt surface to Pt ceride (a) occurs nearly ideally, generating a compact adherent layer, thus confirming the feasibility of the metalliding technique, at least for cases with a large differential in electronegativity as for Ce and Pt. The Al-Ce coating (b) appears more porous than the Pt ceride, particularly nearer to the substrate, and less adhesive. When the substrate is anodically and cathodically polarized, as in Fig. 7, two distinct layers are formed and the adhesion deteriorates, as seen in micrograph (c). The gap between the layers was found to widen (micrograph (d)) for specimens potentiostatically cycled in the more "active" melt, giving voltammograms of Fig. 9, where large anodic currents are superimposed on the reduction currents. Despite the lack of adhesion encountered in metallides obtained below 600°C, it was possible to obtain a coating (micrograph (e)) comparable to that for Pt (micrograph (a)) by immersing Al in a melt comprising $CeCl_3$-LiCl/KCl metallic Ce at 660°C. The Al surface appears to have melted, forming an eutectic with Ce. Except for a few voids, no gap is visible between the coating and the substrate. The diffusion of Ce along grain boundaries into the substrate is clearly apparent from micrograph (e).

Fig. 11   Photomicrographs of Pt after passage of cathodic current in the Ce containing LiCl/KCl melt (a); Al after passing cathodic current (b); Al after passing cathodic and anodic current (c); Al after mainly anodic treatment (as in Fig. 9) (d); Al_3Ce-Al_4Ce on Al (e).

4.1.6   SEM-EDAX Analysis

Film topography varied from granular crystallites to continuous, smooth or rough films. As shown by the SEMs in Fig. 12, the overlayer generally appeared to be crystalline (a), while the underlayer consisted of a black scale (b) over the substrate (c).

Results of EDAX analyses for the various regions are shown in Fig. 13. The crystalline layer (a) is Al-rich, and probably comprises $CeAl_4$. The gap (b) between the layers contains large quantities of Cl in addition to K, Ce and Al. Such a gap was consistently found in specimens that had been anodically polarized, as shown in Fig. 11c and 11d. Composition of the black underlayer (c) varied with the electrochemical treatments, but the intensity of the Al lines was generally lower than that of Ce. This is also apparent from trace (b). Spectrum (d) shows the Al substrate under these layers. Spectrum (e), obtained on a Ce counterelectrode, shows incorporation of Al on the surface.

Although the EDAX analysis in Fig. 13 is representative, the precise ratio of the various components, particularly Cl, varied for the specimens examined. The ratio of relative intensities, Al/Ce was found to vary widely for different samples, and for layers within a sample from 1.2 to 0.2, the higher ratio representing the crystalline outer layer, possibly $CeAl_4$. The less well-defined inner layer generally accompanied large gaps and may comprise more than that one phase, as seen in Fig. 11. The lower Al content in this layer implies a faster diffusion coefficient for Al in Ce than Ce in Al, which suggests variation in the diffusion coefficients of Al in the various intermediary Al-ceride phases.

4.1.7   Microhardness Indentation Tests

Knoop hardness tests performed on the metallided layers and on the Al substrate are compared in Fig. 14. Hardness measurements on the $CeAl_4$-$CeAl_3$ layer averaged 460 HK_{100} compared to 120 HK_{100} for the electroplated and 25 HK_{100} for the Al substrate. Thus, the Al-Ce layer is much harder than either of the component elements.

4.1.8   Discussion of Results of Ceride Formation

Occurrence of several anodic and cathodic reactions between the potentials of Al corrosion (E_{oc}) and Ce deposition ($E_{Ce/Ce^{+3}}$) is evident from voltammetric experiments. Pre-Ce deposition cathodic transitions a, b and c in Fig. 6 at 460, 350 and 20 mV
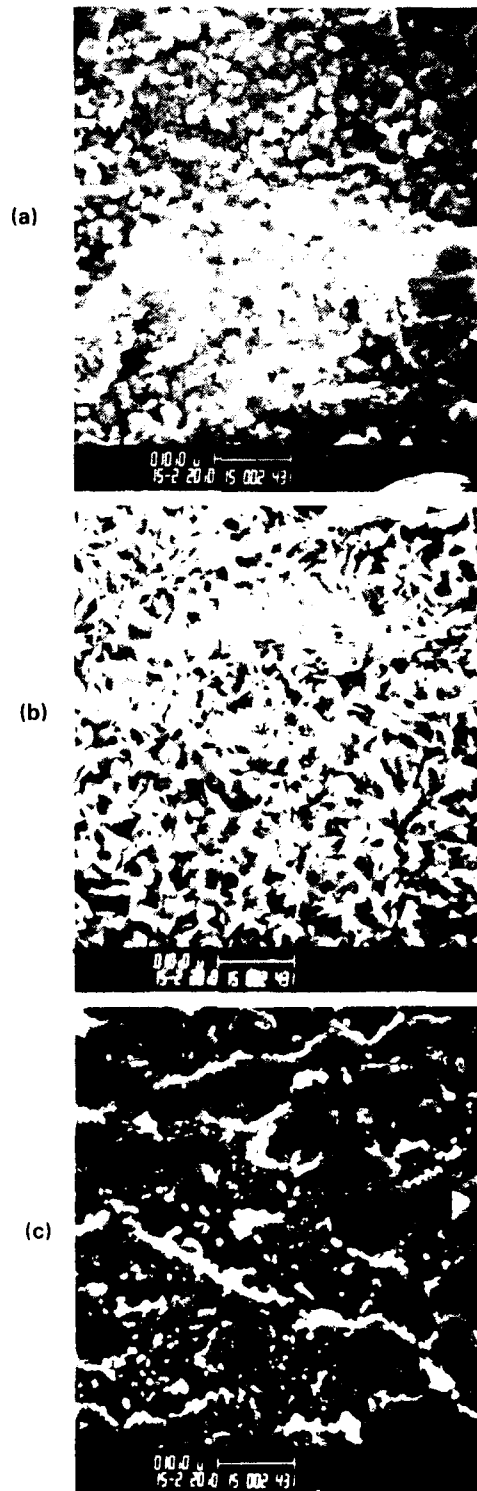
SC85-30048

Fig. 12   SEM of (a) crystalline surface layer, (b) black underlayer on the metallided (c) Al substrate.
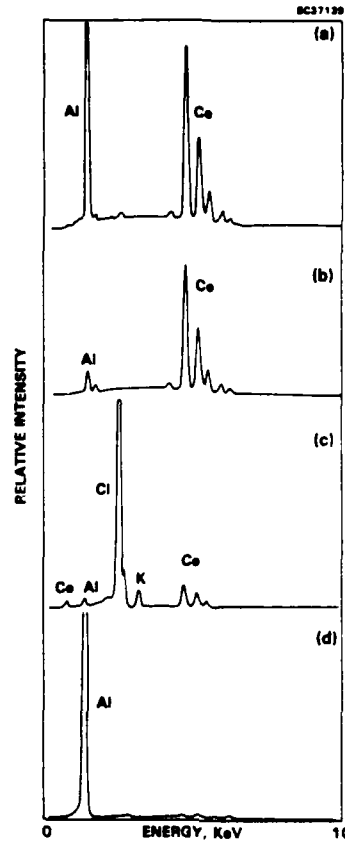
Fig. 13 EDAX for regions a, b, c and d (gap) for the specimens in Fig. 11.

SC34774

120 HK₁₀₀

460 HK₁₀₀

25 HK₁₀₀

⊢─────┤
50 μm

Fig. 14   Photomicrograph of specimen metallided as in Fig. 9, showing indentations for
Knoop hardness tests on the (1) Ce layer, (2) $CeAl_3$-$CeAl_4$ layer, and (3) Al
substrate.

vs $E_{Ce/Ce^{+3}}$, respectively, imply interaction between Al and Ce^+ to form reduced compounds, more anodically stable than Ce. The $CeAl_4$ phase appears to form on Al under a variety of potentiostatic conditions. Minor changes in t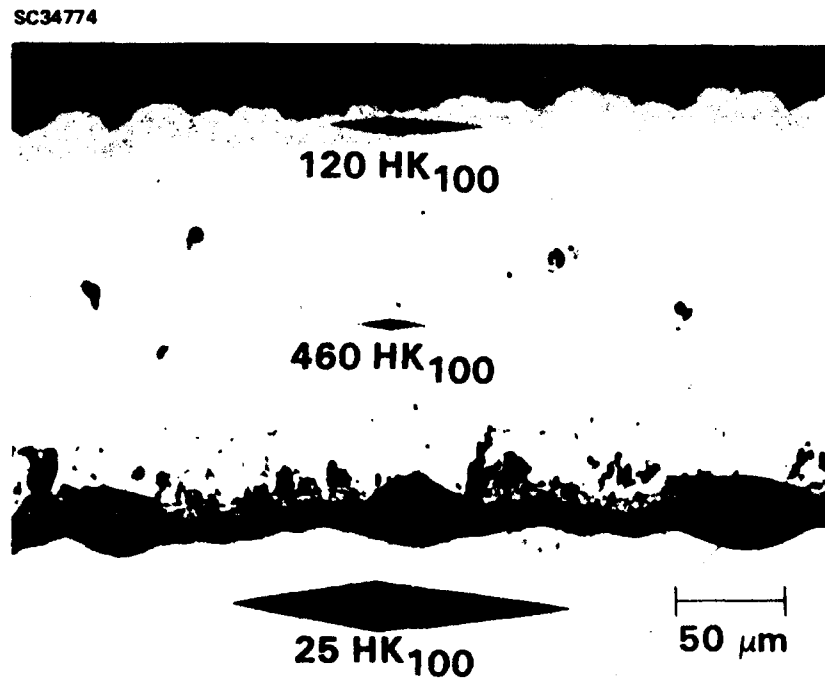he experimental parameters do not affect the stoichiometry of the outer layer, but affect the morphology and adhesion of the coating.

Formation of compounds CeAl, $CeAl_2$, $CeAl_3$ and $CeAl_4$, via reaction

$$mAl + nCe^{+3} + 3ne \rightarrow Ce_nAl_m \tag{7}$$

is a three-electron process. Formation of Ce_3Al involves nine electrons. The respective free energies, ΔG, for processes a, b and c in Fig. 6 are -32, -24 and -14 kcal/mole for a three-electron reduction and -9.5, -7 and -4 kcal/mole for a nine-electron reduction. ΔH_{298} values for $CeAl_4$ and Ce_3Al have been reported to be -39 and -22 kcal/mole, respectively.[10] Thus, while the formation of Ce-Al intermetallics is thermodynamically possible, the formation of Al-rich compounds is more favorable by 10-20 kcal/mole than Ce-rich compounds.

Two possible mechanisms for the formation of the observed $CeAl_3$-$CeAl_4$ layer are: 1) reduction followed by solid-state diffusion of Ce into the Al surface as previously outlined in Eqs. (1)–(4); or 2) reductive precipitation of the $CeAl_3$-$CeAl_4$ compounds from the melt onto the surface of the Al. The experimental results suggest the latter reductive precipitation mechanism.

The reductive precipitation mechanism results in the overall reaction of Eq. (7) by the following steps. First, Al is sufficiently active to dissolve anodically in the Cl^- electrolyte by the reaction:
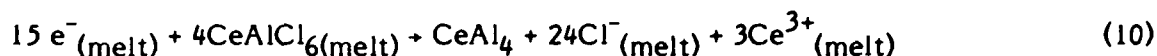
$$6Cl^- + Al_{(metal)} \rightarrow AlCl_6^{3-}{}_{(melt)} + 3e^- \tag{8}$$
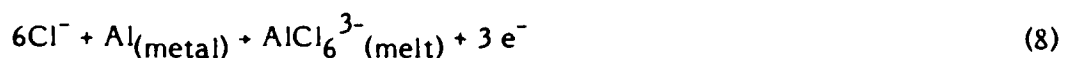
followed by the formation of a Ce chloro-aluminate complex in the melt:

$$AlCl_6^{3-}{}_{(melt)} + Ce^{3+}{}_{(melt)} \rightleftharpoons CeAlCl_{6(melt)} \tag{9}$$
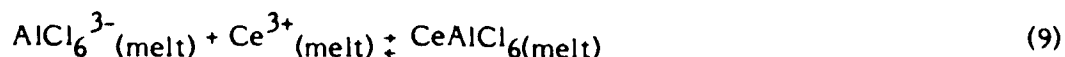
The $CeAlCl_6$ complex is then reduced in the highly reducing, electronically conducting melt to form a $CeAl_4$ precipitate from the melt onto the metal surface as:

$$15\ e^-_{(melt)} + 4CeAlCl_{6(melt)} \rightarrow CeAl_4 + 24Cl^-_{(melt)} + 3Ce^{3+}_{(melt)} \tag{10}$$

This mechanism is consistent with the presence of observed predominant $CeAl_4$ films. Reduction of a Ce chloro-aluminate complex from the melt is also consistent with the observed Cl^- inclusions found in the films. However, after passage of sufficient cathodic charge, a highly reduced intermediate, possibly a Ce(II) complex, builds up in the melt and results in the inclusion of the more reduced $CeAl_3$ compound in the resulting films. This intermediate tends to undergo rapid anodic oxidation, making the melt appear more active (Fig. 9).

The cyclic voltammetric results (Figs. 6-9) support the reductive precipitation mechanism, as shown by the schematic representation of the individual processes in Fig. 15. The dashed-solid curve represents the principal processes in Fig. 6 or 7: the dissolution of Al (i) (Eq. (8)), the precipitation of $CeAl_4$ (b) (Eq. (10)) and reduction of Ce^{+3} (d) (for simplification, transitions a, c, e, f, g and h are not shown). The dotted curve represents the analogous processes indicated by i', b' and d in the more active melt, experiment of Fig. 9, where the predominant anodic process is the oxidation of a highly reduced intermediate, possibly a Ce(II) complex, rather than oxidation of Al to the chloro-aluminate complex (Eq. (8)). The main differences between the two curves is the potential shift for the anodic reaction (j) by ~ 0.5 V due to the presence of the proposed anodically active intermediate in the melt. Superimposition of currents j and b yields a net anodic current i' and a net cathodic current b'.

Additional support for the reductive precipitation model is provided by the abrupt drop in current b, at 0.14 V in Fig. 6, suggesting the formation of a "passivating" film produced by a cathodically generated product.

The formation of Ce-Al metallide via solid-state diffusion must be ruled out, since this reaction requires a high rate for the diffusion of Ce into the Al substrate (k_3 in Eq. (3)). To our knowledge, no data exist in the literature for diffusion coefficients for
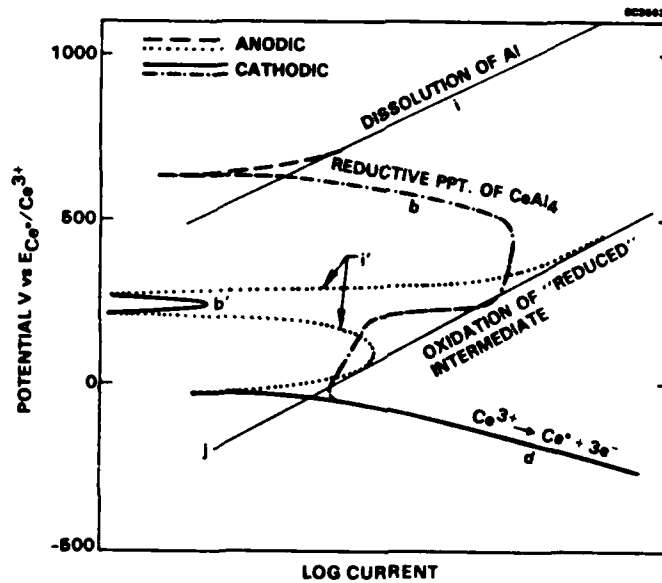
Fig. 15 Schematic representation of the concurrent electrochemical reactions occurring at Al electrodes in Ce-LiCl/KCl melt.

Al in Ce ($D_{Al/Ce}$) or for Ce in Al ($D_{Ce/Al}$). If $D_{Al/Ce} \ll D_{Ce/Al}$, the cerided specimens would have a Ce-rich surface and a [Ce] gradient decreasing exponentially according to Eq. (6) into the bulk. Alternatively, successive phases of Ce_3Al, $CeAl$, $CeAl_2$, $CeAl_3$, $CeAl_4$ and Al would follow a Ce-rich surface. The formation of only one or two Al-rich surface coatings, $CeAl_4$ and $CeAl_3$, and the large gap between and the Al substrate and the coating in Fig. 11 suggest that $D_{Al/Ce} \gg D_{Ce/Al}$.

The solid solubility of Ce in Al is reported as being < 0.5 wt%.[11] The combination of low solubility of Ce in solid Al, the heat of formation of -39 kcal/mole for $CeAl_4$,[10] and probably a high diffusion rate of Al favors the growth of the $CeAl_4$ phase. The formation of these more stable intermetallics, $CeAl_3$ and $CeAl_4$ interferes with the electrodepositon and diffusion of Ce.

The lack of adhesion between the Al substrate and the coating could be attributed to a number of factors, which include: 1) a $D_{Al/Ce} \gg D_{Ce/Al}$; 2) rapid anodic dissolution of Al; and 3) incompatibility of physical properties such as crystal structures,

lattice constants, hardness and temperature coefficients for Al and $CeAl_4$. Factors 1 and 2 are discussed above. The crystal structure of $CeAl_4$ is body-centered tetragonal type, $CeAl_3$ is hexagonal type, and Al is generally cubic face-centered.[11] Indentation tests indicate that the $CeAl_4$-$CeAl_3$ film formed is 20-50 times harder than Al or Ce. Increased tensile strength, hardness, creep strength, and fatigue limit and resistance to elevated temperatures of Al-Ce alloys has been attributed to the presence of inclusions of the hard and brittle compound $CeAl_4$.[12]

Although a hard coating for Al has been developed, ceriding via solid-state diffusion, as in the case of Pt, does not occur. Nevertheless, stable $CeAl_3$ and $CeAl_4$ compounds readily form at temperatures below the melting point of Al. A route other than by electrochemical means may result in adherent wear-resistant layers.

4.2 Formation of Titanides

Potentiostatic and galvanostatic electrolysis of Al 1100 and 1010 steel in LiF/KF containing 1 mole% Ti gave the results summarized in Table 2. Al was more active in the fluoride melt, as evidenced by the negative open-circuit potential vs the Ti reference electrode. For most cases, the Al electrode corroded when polarized at potentials near zero volts vs Ti. For cathodic galvanostatic electrolyses at -50 mA/cm^2 and -5 mA/cm^2, a black salt layer remained on the surface with no apparent deposition of Ti or K.

On steel electrolyzed in the molten Ti-containing bath, electrolysis under very cathodic conditions (-200 mV vs Ti) resulted in apparent plating of Ti without formation of a metallide. EDAX analysis of the resulting surface shows it to be primarily that of Ti (Fig. 16). However, electrolysis at 0 V vs Ti (current equal to 10 mA/cm^2) produced a silvery deposit composed of Ti and Fe shown by the EDAX spectra in Fig. 17a. SEM revealed that the deposit also contained small crystallites composed of Ti and Fe (Figs. 17b and 18). Metallographic cross sections of the specimen (Fig. 19) revealed a thin surface layer having a hardness (KN_{50}) of 170 ± 24 as compared to a substrate hardness of 120 ± 10.

Table 2

Summary of Titaniding Experiments

| T (°C)	Substrate	E mV vs Ti	Conditions	Results
564	Al	-350	Zero V vs Ti ~ 5 mA/cm²	Corrosion
565	Al	-330	-50 mA/cm² galvanostatic	Black layer
560	Al	-290	-5 mA/cm² galvanostatic	Silver white deposit containing K
565	Steel	160	-200 mV vs Ti (~ 50 mA/cm²)	Ti layer under a scale EDAX showed Ti and some K, no Fe
744	Steel	40	0 V vs Ti (~ 10 mA/cm²)	Silver deposit, EDAX showed Ti and Fe
730	Steel	42	0 V vs Ti	Silver deposit, EDAX showed uneven distribution of Fe and Ti
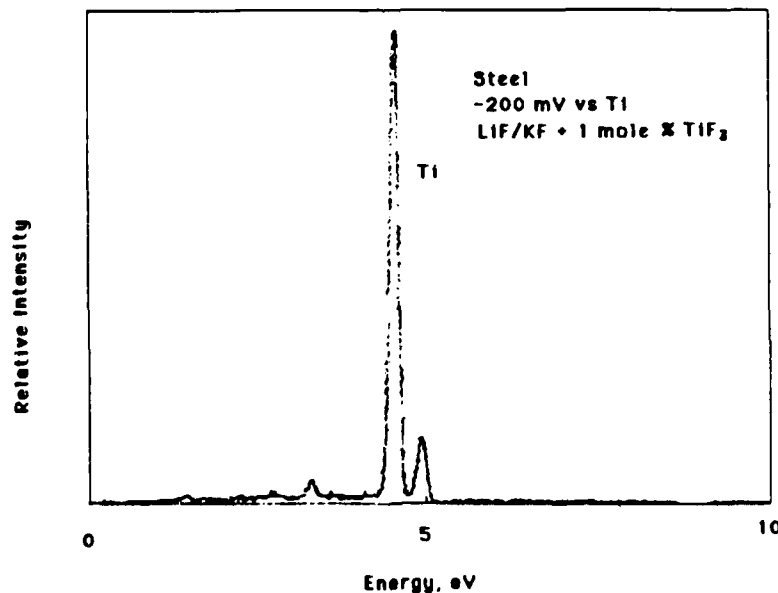
Fig. 16 EDAX for steel surface subjected to electrolysis at -200 mV vs Ti/Ti³⁺ electrode in Ti containing LiF/KF molten salt.
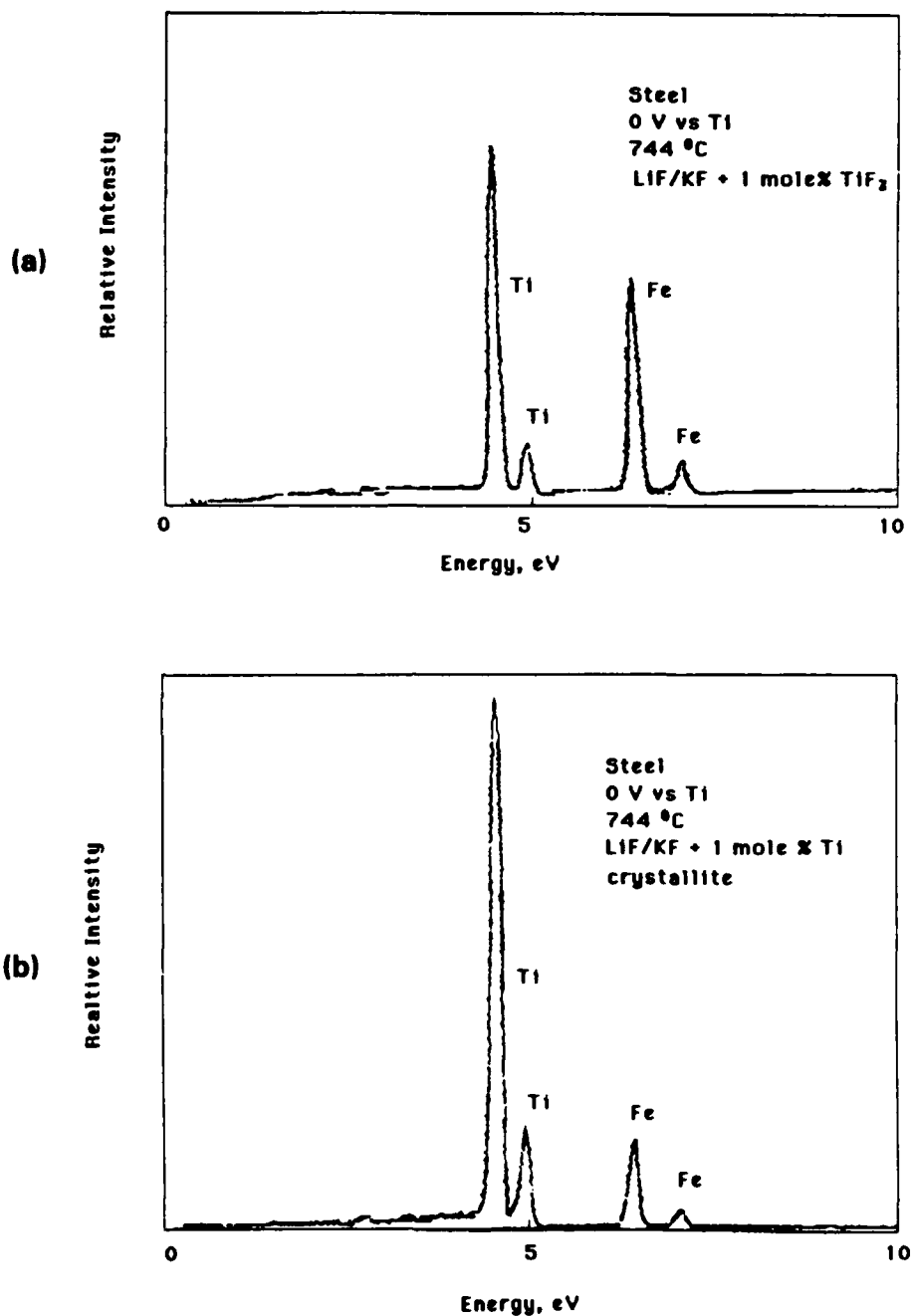
(a)

Steel
0 V vs Ti
744 °C
LiF/KF + 1 mole% TiF$_2$

Ti

Fe

Ti

Fe

Relative Intensity

Energy, eV

(b)

Steel
0 V vs Ti
744 °C
LiF/KF + 1 mole % Ti
crystallite

Ti

Ti

Fe

Fe

Realtive Intensity

Energy, eV

Fig. 17   EDAX for steel surface subjected to electrolysis at 0 V vs Ti/Ti^{3+} electrode
(10 mA/cm^2) in Ti containing LiF/KF molten salt at 744°C (a); crystallite
formed under the same conditions (b).

SC39149

STEEL
LiF/KF BATH CONTAINING 1 MOLE% TiF_3
744°C
+40 mV vs Ti

Fig. 18 SEM of Ti-Fe crystallite.

SC39148

STEEL
LiF/KF BATH CONTAINING 1 MOLE% TiF_3
774°C
+40 mV vs Ti

Fig. 19 Metallograph of a Ti-Fe coated steel.

4.3 Formation of a Borided Surface

The electrochemical formation of borided steel has been reported elsewhere[5] and reproduced here. A galvanic current of 12 mA/cm^2 for 51 min produces a nominally 400 μm layer shown in Fig. 20 having a Knoop hardness (100 g load) between 1100-1300, which is ten times that of the substrate (KN^{100} = 106).

Using similar and higher currents, no boriding of Al was achieved. Figure 21 shows the current vs voltage behavior for the steel and Al substrates in the boron-containing melt. The potential vs a carbon pseudo-reference electrode was swept at a rate of 10 mV/s. The current densities are very high and of the same order of magnitude for both materials. The zero current potential E_{oc} for steel is much more positive than that for the more active Al by about 1 V. A large change in the cathodic overvoltage appears for the steel electrode after the first sweep in the cathodic direction. For Al, an

SC38922

STEEL
LiF/KF MELT CONTAINING 3.5 MOLE% KBF$_4$
−12 mA/cm^2 FOR 51 MINUTES
886°C

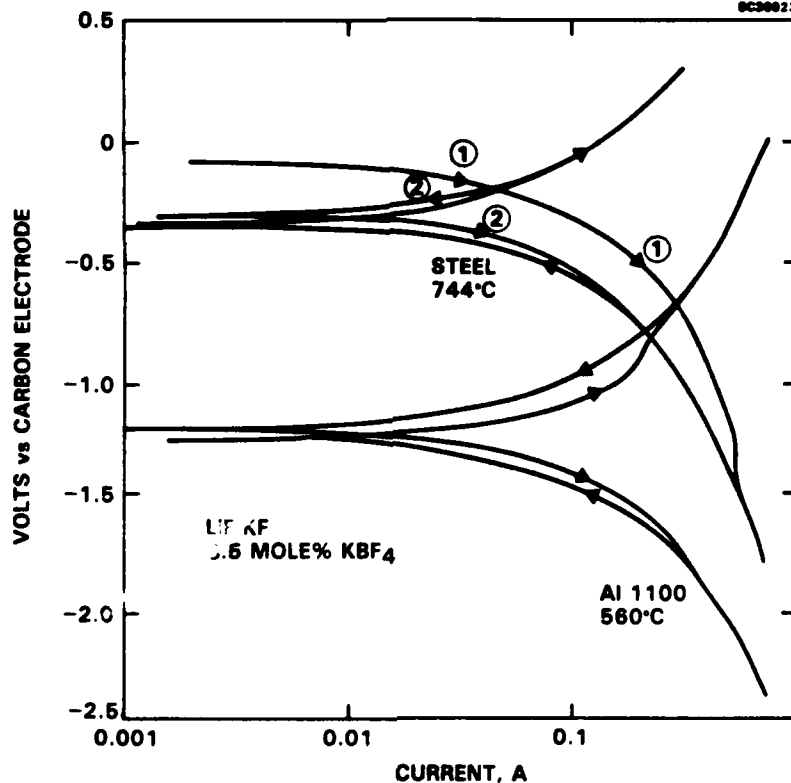Fig. 20 Photomicrograph of a borided steel surface.

Fig. 21   Current vs potential behavior for steel at 744°C and Al at 560°C in a LiF/KF
melt containing 3.5 mole% BF_4-.

apparent increase in anodic current occurs after the cathodic scan, indicating a reversible redissolution of a cathodically deposited material.

Electrochemical impedance for Al at open circuit in the boron-containing melt, Fig. 22, shows an R_p of 4.54 Ω cm^2 which corresponds to an exchange current density in the vicinity of 5 mA/cm^2. Note from the high-frequency limit for the impedance spectrum that the solution resistance is also quite high, equal to 4.46 Ω, comparable to the polarization resistance. The high-solution resistance shows that it is difficult to accurately potentiostat the test surface due to high ohmic drops, and hence all electrolyses were performed galvanostatically.

The electrochemical analyisis provides some insight into why boriding occurs for steel, but not Al. While the electrochemical reactions occurring on steel at 744°C and Al at 560°C in the boron-containing fluoride melts appear to be comparable and rapid (exchange current densities on the order of 5 mA/cm^2), the reactions giving rise to
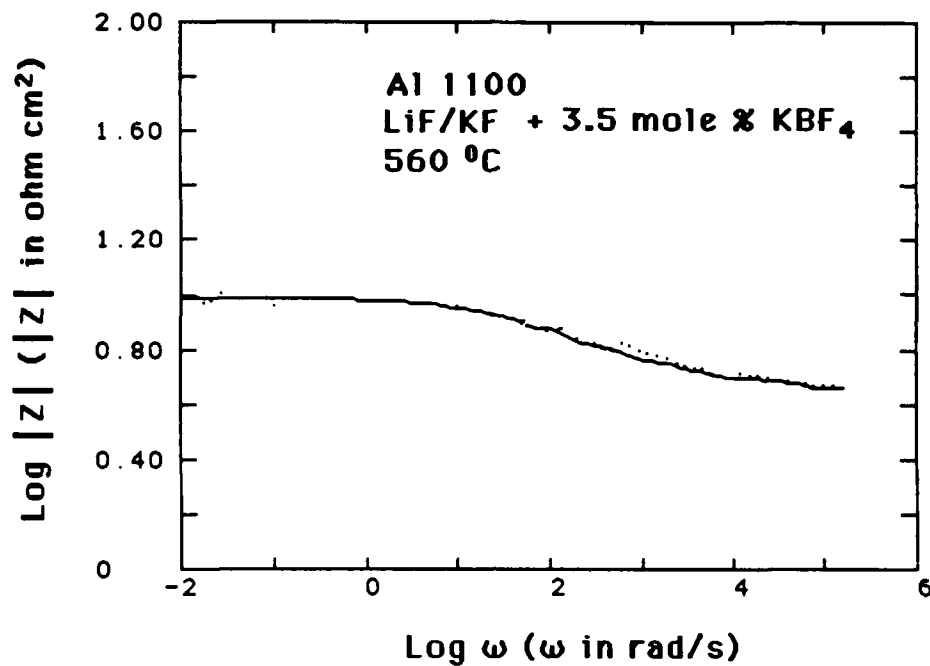
32

Fig. 22 Log impedance modulus vs log frequency for a steel electrode in a LiF/KF melt containing 3.5 mole% BF_4^-.

these current densities are no doubt quite different. On Al, the reactions entail the anodic dissolution of Al metal to form Al fluoride complexes and reduction of the Al and boron complexes. Steel, on the other hand, is sufficiently inert such that the corrosion reaction is relatively low, as evidenced by the lack of current hysteresis upon reoxidation (Fig. 21). The reaction that depolarizes the steel interface is the metalliding reaction (Eq. (2)). It can be concluded that Al in the boron-containing melt is too active from a corrosion standpoint to allow the metalliding reaction to take place.

4.4 Corrosion Protection of Steel

From the previous results, it is seen that titaniding increases the hardness of the surface by about 30%, while the borided steel surface has an increase in hardness over the substrate by a factor of 10. These increases in mechanical properties are advantageous with respect to the wear behavior of the materials, but overall improvement of materials properties for adverse environments must also include consideration of the corrosion protective behavior of the surface formed by surface modification. Hence,

the corrosion behaviors of the borided and titanided steel were determined in neutral chloride. This environment was chosen since it represents a realistic environment that a structural material would experience as exposed to the atmosphere. Usually, corrosion evaluation of materials entails accelerating the process and observing the results either by gravimetric analysis or by electrochemical means. For example, the test piece is often placed in a sulfuric acid electrolyte and polarized in the anodic direction. This accelerates certain anodic reactions, but possibly not those relevant to the reactions that occur in near-neutral media and under open-circuit conditions, as would be expected for atmospheric conditions. Hence, the corrosion behavior of the surface treated steels were evaluated at their corrosion potential, E_{corr}, in aerated, room-temperature 0.5 M NaCl using electrochemical impedance spectroscopy. Figures 23 and 24 show the spectra for the titanided and borided steels.

The spectra for the borided steel exposed to 0.5 M NaCl show very little change with exposure over a 48 h test period. At the end of the test, the surface had a layer of orange ferric corrosion product. The corrosion resistance, R_p, and the capacitance, C_p, were evaluated assuming the electrochemical impedance followed the equation:

$$Z = R_s + R_p/(1 + (j\omega R_p C_p)^\alpha \tag{11}$$

where C_p is an apparent capacitance, $j^2 = -1$, R_s the ohmic contact resistance, ω the frequency in rad/s, and α is a unitless phenomenological parameter.[13] This equation approximates the frequency response typically observed for the corrosion of steel in neutral media where the corrosion rate is determined by the blocking of the diffusion-controlled oxygen reduction by a surface layer.[14] R_p relates directly to the corrosion current density, I_o, as

$$I_o = B/R_p \tag{12}$$

where B is a phenomenological coefficient. Assuming a B value of 20 mV,[15] the calculated corrosion rate for the borided steel is 2×10^{-5} amp/cm^2. R_p varies slowly with time decreasing slightly from an initial value over 1000 Ω-cm^2 after 48 h exposure. R_p for 4340 steel[14] shows a similar behavior (Fig. 25a). The capacitance for the borided
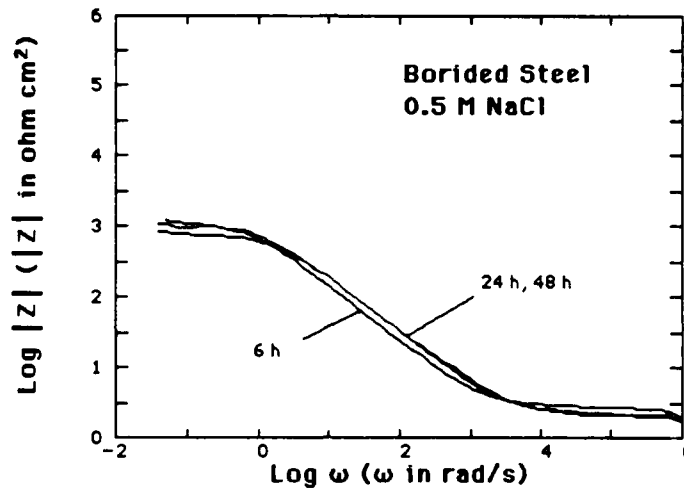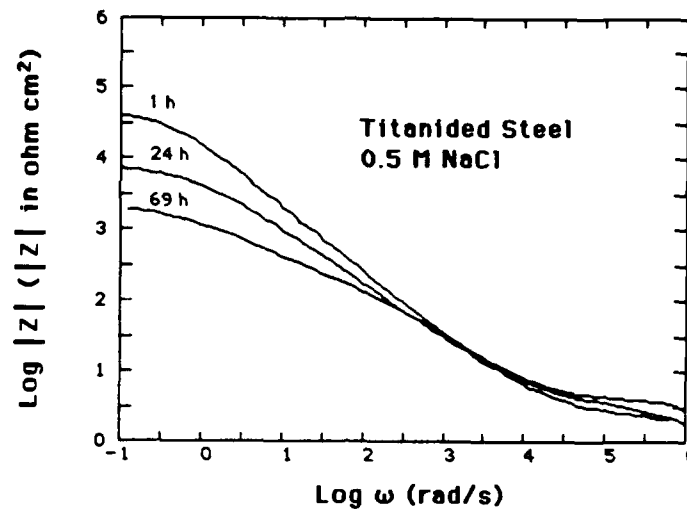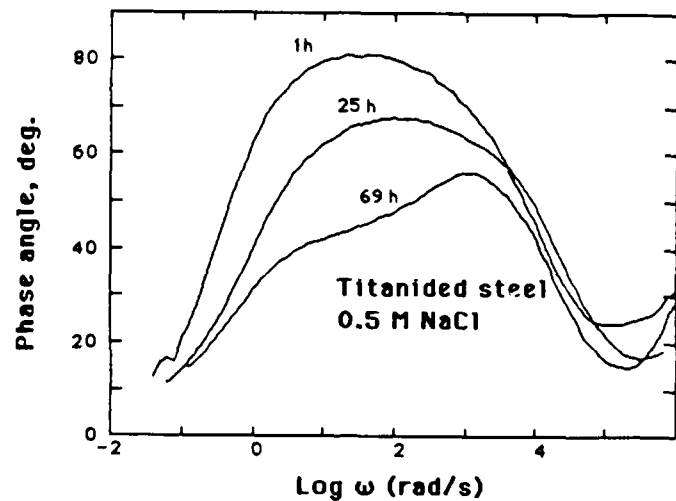
(a)
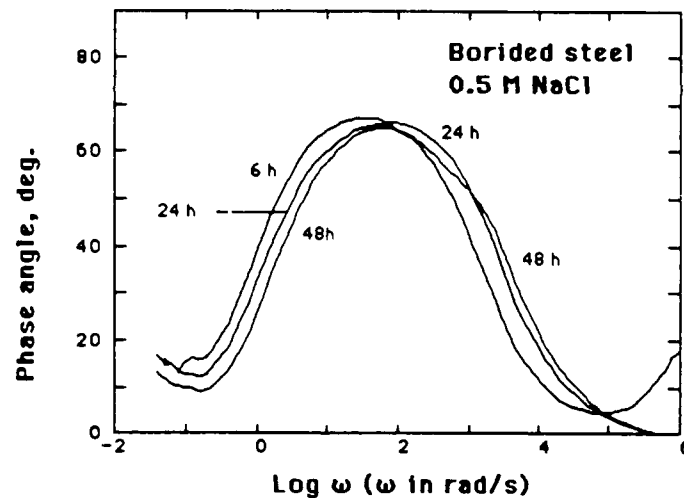
(b)

Fig. 23   Log impedance modulus (a) and phase angle (b) vs log ω for carbon steel borided in a LiF/KF melt containing 3.5 mole% B for 51 min at a current density of 12 mA/cm². Curves taken as a function of exposure to aerated, room-temperature 0.5 M NaCl.

(a)

(b)

Fig. 24   Log impedance modulus (a) and phase angle (b) vs log ω for carbon steel titanided at 0 V vs Ti in a LiF/KF melt containing 1 mole% Ti. Curves taken as a function of exposure to aerated, room-temperature 0.5 M NaCl.

steel, however, decreases with time (Fig. 25b), suggesting the slow formation of a blocking film, and the corrosion potential shows a slight increase with time (Fig. 25c). These trends are significantly different from the 4340 steel (Fig. 25b,c), suggesting that for longer times, boriding might to some degree protect the steel against corrosion.

While the corrosion behavior of the borided steel is quite similar to that of 4340 steel in stagnant 0.5 M NaCl, the titanided carbon steel shows a comparatively large improvement in corrosion resistance over an approximate 70 h test period. Initially, R_p obtained from the impedance spectra of the titanided carbon steel (Figs. 24 and 25a) exceeds 3×10^4 Ω-cm^2 and decreases to 2000 Ω-cm^2 after 69 h exposure to the 0.5 M NaCl (Figs. 24 and 25a). E_{corr} for the titanided specimen is significantly higher as compared to the borided carbon steel and the 4340 specimen. After 69 h exposure, the phase-angle spectrum for the impedance of the titanided steel (Fig. 24b) exhibits the onset of a second time constant, which may relate to the localized corrosion and undercutting of surface-modified regions. After 69 h exposure, only a single corrosion spot was observed on the titanided specimen.

These results show that metalliding can improve the corrosion resistance. Although the borided steel shows a corrosion rate comparable to untreated 4340 in stagnant 0.5 M NaCl over 48 h exposure, a decrease in the observed capacitance of the borided steel with time and a corresponding increase in the corrosion potential suggest that the long-term durability of the material may be slightly better than that for 4340, possibly as a result of the formation of a more highly blocking protective corrosion product layer owing to a surface buffering by the presumed borate component of the corrosion product. The titanided steel, while not showing as great an improvement in hardness over the substrate as does the borided steel, exhibits a significant improvement in the corrosion resistance as compared to both 4340 steel and the borided steel for the 69 h exposure to 0.5 M NaCl. Corrosion of the titanided specimen presumably occurs at defects in the surface layer.
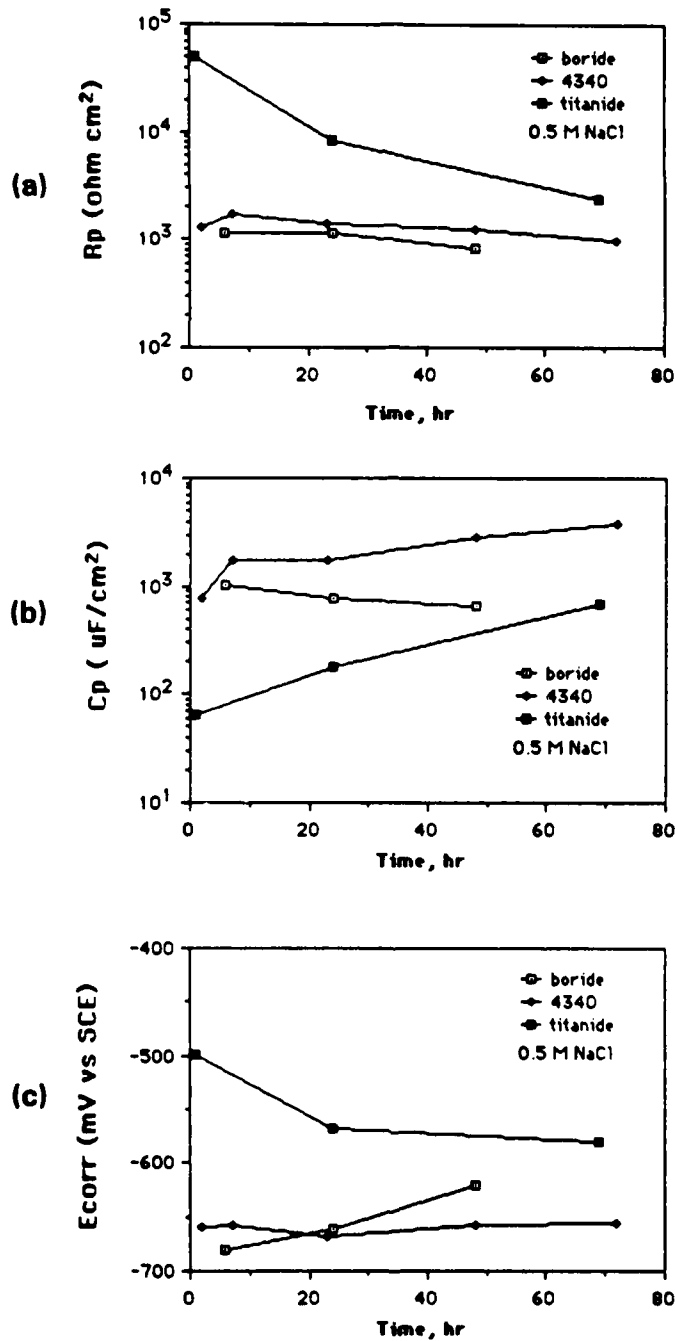
Fig. 25 Time dependence for (a) the corrosion resistance, (b) the capacitance, and (c) corrosion potential for borided, titanided steel and 4340 steel in aerated 0.5 M NaCl.

5.0 BIBLIOGRAPHY

1. N.C. Cook, Scientific American, 38 (1969).

2. R.S. Sethi, J. Appl. Electrochem. 9, 411 (1979).

3. I.F. Danzig, R.M. Dempsey and A. B. Conti, Corrosion 27, 55 (1971).

4. J.C. Withers, J. E. Perry and B.A. Fosnocht, Techn. of Metals Research, Vol. 7, R.F. Bunshah, ed., 1972.

5. H. Fiedler, R. Sieraski, Met. Progr. 99 (2), 101 (1970).

6. N. Cook and W.J. Hayes, Ger. Offen. 1,933,010; Chem. Abstr. 72, 74037A (1970).

7. M. Kendig, A. Allen and F. Mansfeld, J.Electrochem. Soc. 131 (4), 935 (1984) and references therein.

8. M. Kendig, A.T. Allen and F. Mansfeld, Corrosion 85, R. Baboian, ed. (to be published).

9. F. Mansfeld, Corrosion 37, 301 (1981).

10. W. Blitz and H. Priper, Z. Anorg. Allg. Chemie 134, 13 (1924).

11. H. Nowoty, Zertschr. Metallkunde 34, 22 (1942).

12. C. Arens, Metals and Alloys 22, 749 (1945).

13. M. Kendig and F. Mansfeld, Corrosion 39, 466 (1983).

14. J. Juttner, F. Mansfeld and M. Kendig, "Frequency Response Analysis of Transport-Controlled Electrod Processes on Partially Blocked Surfaces," SCTR-85-4, unpublished manuscript, Rockwell Science Center, 1985.

15. F. Mansfeld, "The Polarization Resistance Technique for Measuring Corrosion Currents," Chapter 3, Advances in Corrosion Science and Technology," M. Fontana and R. Staehle, eds., Vol. 6, Plenum Press, NY (1970).

6.0 PUBLICATIONS

M. Kendig, "Metalliding as an Electrochemical Process," Interim Report, SC5398.IN, Rockwell International Science Center, April 1985.

S. Menezes, S. Jeanjaquet, D. Raleigh and M. Kendig, "Electrochemical Formation of Aluminum Ceride on Aluminum," submitted to J. Electrochem. Soc.

M. Kendig, S. Menezes and S. Jeanjaquet, "Corrosion Resistance of Borided and Titanided Steel," technical note to be submitted to Corrosion.

7.0 PARTICIPATING SCIENTIFIC PERSONNEL

M. Kendig, D. Raleigh, S. Jeanjaquet, S. Menezes and D. Wong.

END

5-87

DTIC